JACS
JOURNAL OF THE AMERICAN CHEMICAL SOCIETY

ARTICLE

pubs.acs.org/JACS

CO Oxidation on Inverse CeO_x/Cu(111) Catalysts: High Catalytic Activity and Ceria-Promoted Dissociation of O_2

Fan Yang,[†] Jesús Graciani,[‡] Jaime Evans,[§] Ping Liu,[†] Jan Hrbek,[†] Javier Fdez. Sanz,[‡] and José A. Rodriguez*[,†]

[†]Chemistry Department, Brookhaven National Laboratory, Upton, New York 11973, United States

[‡]Departamento de Química Física, Facultad de Química, Universidad de Sevilla, E- 41012 Sevilla, Spain

[§]Facultad de Ciencias, Universidad Central de Venezuela, Caracas 1020-A, Venezuela

ABSTRACT: A Cu(111) surface displays a low activity for the oxidation of carbon monoxide ($2CO + O_2 \rightarrow 2CO_2$). Depending on the temperature, background pressure of O_2, and the exposure time, one can get chemisorbed O on Cu(111) or a layer of Cu_2O that may be deficient in oxygen. The addition of ceria nanoparticles (NPs) to Cu(111) substantially enhances interactions with the O_2 molecule and facilitates the oxidation of the copper substrate. In images of scanning tunneling microscopy, ceria NPs exhibit two overlapping honeycomb-type moiré structures, with the larger ones (H_1) having a periodicity of 4.2 nm and the smaller ones (H_2) having a periodicity of 1.20 nm. After annealing CeO_2/Cu(111) in O_2 at elevated temperatures (600−700 K), a new phase of a Cu_2O_{1+x} surface oxide appears and propagates from the ceria NPs. The ceria is not only active for O_2 dissociation, but provides a much faster channel for oxidation than the step edges of Cu(111). Exposure to CO at 550−750 K led to a partial reduction of the ceria NPs and the removal of the copper oxide layer. The CeO_x/Cu(111) systems have activities for the $2CO + O_2 \rightarrow 2CO_2$ reaction that are comparable or larger than those reported for surfaces of expensive noble metals such as Rh(111), Pd(110), and Pt(100). Density-functional calculations show that the supported ceria NPs are able to catalyze the oxidation of CO due to their special electronic and chemical properties. The configuration of the inverse oxide/metal catalyst opens new interesting routes for applications in catalysis.

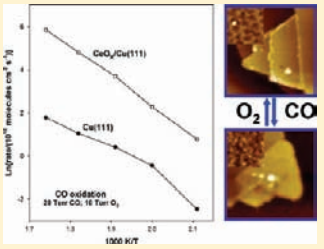

1. INTRODUCTION

Oxidation of carbon monoxide ($2CO + O_2 \rightarrow 2CO_2$) over copper catalysts is significant for understanding fundamental processes associated with methanol synthesis, the water−gas shift reaction, the reforming of alcohols, the operation of fuel cells, and automotive exhaust controls, to mention a few major applications in the area of catalysis.[1−5] In automotive exhaust emission control, the complete oxidation of carbon monoxide is of prime importance to meet increasingly stringent environmental regulations in a practical way.[5,6] Furthermore, since the classic studies of Langmuir, CO oxidation on metal and oxide surfaces is often viewed as an ideal reaction for fundamental investigations in heterogeneous catalysis.[7] For a long time, precious metals have been used as catalysts for CO oxidation.[7−10] These systems can undergo rapid deactivation due to the presence of small amounts of impurities. Owing to the high cost and less abundance of noble metals, noble metal-free catalysts have been explored lately.[5,6] Especially, copper and copper-based catalysts have been the focus of much attention because of their superior catalytic activity toward the oxidation of CO in regular and hydrogen-rich (PROX) streams.[2,5,6,11−13]

Ceria, CeO_2, is widely used as a support for current state-of-the-art CO oxidation catalysts.[2,5,11,13] In general, the high activity of CuO/CeO_2 catalysts for the oxidation of CO is attributed to strong interaction between CuO and the CeO_2 support but the exact role of ceria in these systems is not known.[5] Ceria exhibits two features that make it an interesting material for use as a support in redox catalysts.[14] First, it has the ability to shift easily between Ce^{4+} and Ce^{3+} oxidation states depending on whether it is present in an oxidizing or reducing atmosphere. And second, it contains numerous oxygen vacancies within its structure leading to high oxygen mobility.[14] A recent study has shown the superior performance of an inverse CeO_2/CuO powder catalyst during the oxidation of CO.[12] As shown in Scheme 1, an inverse oxide/metal catalyst exposes oxide nanoparticles, NPs, to the reactants. Defect sites present in the oxide are not covered by metal particles, as in the case of a traditional metal/oxide catalyst.[7c,d,15−17] In the inverse catalyst, the reactants can interact with defect sites of ceria NPs, metal sites of the support, or the metal−oxide interface.[15] Thus, one can gain activity due to the active participation of ceria in the catalytic reaction.[7c,d,15−17]

In this article, we use well-defined CeO_x/Cu(111) surfaces to investigate the behavior of inverse CeO_2/CuO catalysts. Scanning tunneling microscopy (STM) allows us to monitor changes in the morphology of the CeO_x/Cu(111) surfaces before and after reaction with CO and O_2. It is known that exposure of Cu(111) to O_2 induces the formation of a distorted Cu_2O(111)-like layer,[18−20,22] which has the same honeycomb structure as that of the (1 × 1)-Cu_2O(111) surface, but with coordinatively under-saturated Cu atoms removed.[18−21] The present studies indicate that CeO_x nanoparticles deposited on Cu(111) have special structural and electronic properties that facilitate the dissociation of the O_2 molecule. Oxygen spills from the ceria nanoparticles onto the copper substrate forming films of Cu_2O

Received: September 29, 2010
Published: February 22, 2011

dx.doi.org/10.1021/ja1087979 | J. Am. Chem. Soc. 2011, 133, 3444–3451

Scheme 1

and Cu_2O_{1+x}. Although Cu(111) has a poor catalytic activity for the oxidation of CO, the $CeO_x/Cu_2O_{1+x}/Cu(111)$ surfaces are more catalytically active than surfaces of noble metals such as Pt(100) and Pd(110).

2. EXPERIMENTAL AND THEORETICAL METHODS

2.1. Microscopy, Photoemission, and Catalytic Tests. The STM experiments were carried out in a ultrahigh vacuum (UHV) chamber with a base pressure $<1 \times 10^{-10}$ mbar and equipped with an Omicron variable-temperature STM, surface cleaning facilities, and a Focus e-beam metal evaporator.[16,17] The copper substrate temperature was measured by a K-type thermocouple, which was installed on a linear motion feedthrough and pressed against the top of the sample surface.[17] A resistive heater positioned at the back of the sample could increase the sample temperature up to 1000 K. The Cu(111) sample was cleaned by repeated cycles of Ne sputtering (2 keV, 40 min) and annealing (800 K, 10 min).[16] Chemically etched W tips were used for imaging the surface. Ce atoms were evaporated by e-beam heating Ce foils (>99.9% purity) housed in a Ta crucible. In these experiments, Ce atoms were always evaporated onto the Cu(111) surface in an oxygen atmosphere, typically 5×10^{-7} mbar O_2, to prevent the alloying between Cu and Ce metal atoms.

Photoemission studies were performed at beamline U7A of the National Synchrotron Light Source (NSLS) at Brookhaven National Laboratory using a photon-energy of 625 eV to collect the O 1s region, and 325 eV to collect the Ce 4d and valence regions. In a separate UHV chamber, we acquired XPS spectra (Ce 3d, O 1s, and Cu 2p regions) and UPS spectra (valence region) using Mg Kα and He−I radiation, respectively. The core-levels of Ce display quite different features for Ce^{3+} and Ce^{4+} oxidation states.[16,23] Curve-fitting of the Ce 3d XPS spectra[16] allowed us to determine the ratio of Ce^{3+}/Ce^{4+} in the ceria overlayers. The area of the copper surface covered by ceria was estimated using STM images or a combination of ion scattering spectroscopy (ISS) and XPS.[17] Before the ISS measurements, the $CeO_x/Cu(111)$ surfaces were exposed to CO in order to remove the Cu_2O and expose the fraction of the copper surface not covered by ceria.[17]

The catalytic studies were carried out in a system which combines a batch reactor and a UHV chamber.[8,16,17] The sample could be transferred between the reactor and UHV chamber without exposure to air. Typically, it was transferred to the batch reactor at ~298 K, then the reactant gases were introduced (20 Torr of CO and 10 Torr of O_2). The catalytic activity for CO oxidation was measured at 475−575 K.[24] Product yields were analyzed by gas chromatography or mass spectroscopy.[8,16,17] The amount of molecules produced was normalized by the active area exposed by the sample. In our reactor, a steady-state regime for the oxidation of CO was reached after 2−3 min of reaction time.

2.2. Density Functional Calculations. Theoretical calculations have been performed using the plane-wave density functional theory, DFT, approach within the projector augmented wave method (PAW)[25] together with the GGA exchange correlation functional proposed by Perdew et al.[26] as implemented in the VASP 4.6 code.[27,28] A plane-wave cutoff energy of 400 eV was used. We treated the Cu (3d, 4s), Ce (4f, 5s, 5p, 5d, 6s), C (2s, 2p), O (2s, 2p), and H (1s) electrons as valence states, while the remaining electrons were kept frozen as core states. To obtain faster convergence, thermal smearing of one-electron states ($k_BT = 0.05$ eV) was allowed using the Gaussian smearing method to define the partial occupancies. To represent adequately the electronic structure of Ce (in particular the 4f level of the Ce^{3+} species), we used the DFT+U formalism. The Hubbard U term was added to the plain GGA functional employing the rotationally invariant approach proposed by Dudarev et al.,[29] in which the Coulomb U and exchange J parameters are combined into a single parameter $U_{eff} = U - J$. For Ce, we have used the U_{eff} of 4.5 eV which was calculated self-consistently by Fabris et al.[30] using the linear-response approach of Cococcioni et al.,[31] and which is in the range of values usually proposed in the literature (4.5−5.5 eV) for GGA calculations.[32−40] We have used successfully this value for supported NPs of CeO_x in our previous work.[8,17]

To describe the Cu(111) surface, a four-layer thick model slab was used. To avoid lateral interactions, the calculations were carried out using a relatively large $(4\sqrt{3} \times 4\sqrt{3})$ supercell (192 Cu atoms) including a vacuum 15 Å thick. Following our previous work,[17] we modeled the CeO_x NPs supported on Cu(111) using clusters of 6 Ce atoms that we added to only one side of the slab. In the geometry optimizations, two Cu layers of the bottom were kept frozen at the optimized bulk positions.

3. RESULTS AND DISCUSSION

3.1. Reaction of O_2 with Cu(111). Figure 1 shows STM images recorded after adsorbing different amounts of oxygen on Cu(111). Depending on the temperature, background pressure of O_2, and the exposure time, one can get chemisorbed O on Cu(111) or a layer of Cu_2O that may be deficient in oxygen.[18−22] In the first stages of oxidation, Figure 1B, one finds the formation of an O-deficient $Cu_2O(111)$ layer. The brightest dots in Figure 1B denote the presence of O vacancies in the Cu_2O surface oxide. This is followed by the formation of the so-called

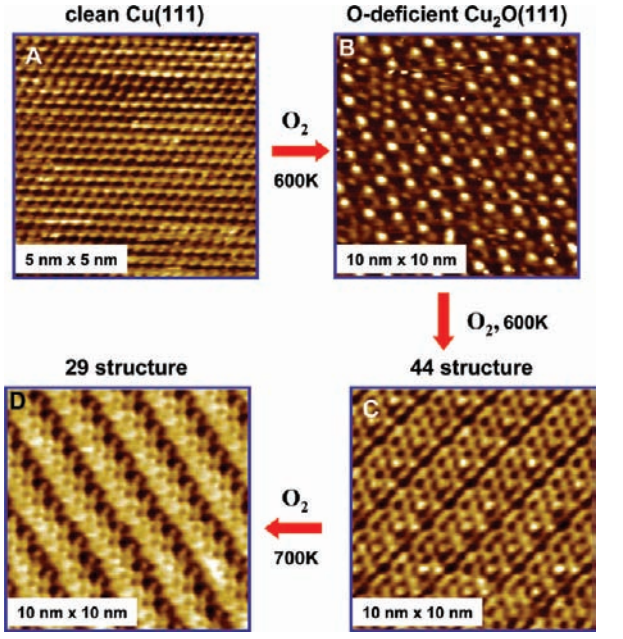

Figure 1. STM images of structures for the Cu_2O oxide film formed during the oxidation of Cu(111). (A) Clean Cu(111); (B) O-deficient $Cu_2O(111)$, formed by annealing Cu(111) in 5×10^{-7} Torr O_2 at 600 K for less than 10 min; (C) a '44' structure of Cu_2O surface oxide, formed by annealing Cu(111) in 5×10^{-7} Torr O_2 at 600 K for 20 min; and (D) a '29' structure of Cu_2O surface oxide, formed by annealing Cu(111) in 5×10^{-7} Torr O_2 at 700 K for 20 min.

dx.doi.org/10.1021/ja1087979 |J. Am. Chem. Soc. 2011, 133, 3444–3451

"29" and "44" structures.[19−21] Figure 1C displays the structure of a Cu_2O surface layer which has unit cell vectors of 2.20 and 1.18 nm. Since the unit cell of the surface oxide is 44 times larger than the (1×1) unit cell of Cu(111), this oxide surface layer is often referred to as the "44" structure in previous studies on the oxidation of Cu(111).[18−22] A structural model for this Cu_2O/Cu(111) system has been proposed by Jensen et al.[19,20] and Matsumoto et al.[18] These authors suggest that the "44" structure originates from a distorted Cu_2O(111)-like layer grown epitaxially on the Cu(111) substrate. The Cu_2O(111)-like layer has the same honeycomb structure as that of the (1×1)-Cu_2O(111) surface, but with coordinatively under-saturated Cu atoms (*cus*-Cu) removed.[18−20] The structure in Figure 1C was formed by annealing Cu(111) in 5×10^{-7} Torr of O_2 at 550−650 K for 20 min (see caption with the corresponding exposure times). Exposure to O_2 at higher temperatures (700−750 K) leads to formation of the "29" structure in Figure 1D. The formation of the ordered "44" and "29" structures marks the end of the surface oxidation of Cu(111) with $P_{O2} < 10^{-5}$ Torr.[22] Further oxidation in the same temperature range does not lead to changes of surface morphologies. Correspondingly, XPS measurements showed that the O 1s intensity reached a maximum value at 650 K and ≥600 L O_2 exposure. The existence of a saturation in surface oxygen coverage is consistent with previous studies of Auger electron spectroscopy (AES)[20,41] on the oxidation of Cu(111).

3.2. Reaction of O_2 with CeO_x/Cu(111): Ceria Promoted Oxidation of Copper. The addition of ceria NPs to Cu(111) enhances interactions with the O_2 molecule and facilitates the oxidation of the copper substrate. Nano-sized ceria islands supported on the Cu(111) surface were synthesized by vapor deposition of cerium atoms in O_2 onto the Cu(111) surface at elevated temperatures.[17] The first panel in Figure 2 shows a ceria island deposited in 5×10^{-7} Torr O_2 at 550 K. The ceria NP is located at an ascending step edge and surrounded by Cu_2O surface oxides. In region A, the Cu_2O surface oxide has a hexagonal lattice with a periodicity of 0.60 nm, which corresponds to the structure of the ordered (1×1)-Cu_2O(111) phase. Further away from the ceria island, region B, the structure of the Cu_2O surface oxide is characteristic of the structure of the O-deficient Cu_2O(111) phase, and large bright spots denote oxygen vacancies, which has been observed and identified in our studies on the oxidation (Figure 1B) and reduction of Cu(111).[22] The smaller O coverage further away from the ceria island suggests that O_2 dissociation occurs at the ceria sites. Dioxygen dissociation also occurs on Cu(111) at elevated temperatures.[18,20,22] Matsumoto et al.[18] have shown that Cu_2O surface oxides grow from the steps of Cu(111) at above 500 K. Since the formation of a Cu_2O surface oxide is limited by the rate of O_2 dissociation, we could use surface areas of the Cu_2O surface oxide as a reference to compare the rate of O_2 dissociation at ceria sites with that at the step edge of Cu(111). In Figure 2, while the Cu_2O oxide growing from the step covers a small portion of surface, the majority of the Cu(111) surface terraces has been covered by the Cu_2O surface oxide growing from around ceria islands. Therefore, Figure 2 illustrates that ceria NPs are not only active for O_2 dissociation, but provide a much faster channel than the step edges of Cu(111) for the dissociation of O_2. As we will see in section 3.5, this is a consequence of the unique electronic and chemical properties of the ceria NPs.

Interestingly, the presence of ceria on Cu(111) leads to the formation of a novel surface oxide phase of Cu_2O at extended O_2 exposure. Figure 3 shows that, after annealing the CeO_2/Cu(111) surface in 5×10^{-7} Torr O_2 at 700 K, a new phase of Cu_2O_{1+x} surface oxide appears. Previous oxidation studies of Cu(111) had shown that an ordered Cu_2O-like layer is formed on Cu(111) in $<10^{-4}$ Torr O_2, with a characteristic "29" structure at 700 K (Figure 1D).[18−22] In the presence of ceria NPs, we observed the formation of the "29" structure, as well as a few other intermediate structures, which eventually transformed into a new Cu_2O_{1+x} surface oxide phase. The height of the bright rows in Figure 3A suggests that there is an overlayer oxide growth, as opposed to the single layer of Cu_2O surface oxide observed in Figure 1. This is consistent with the fact that the intensity of the O 1s signal in XPS was substantially (~3 times) larger after dosing O_2 to the CeO_x/Cu(111) surface. As shown in

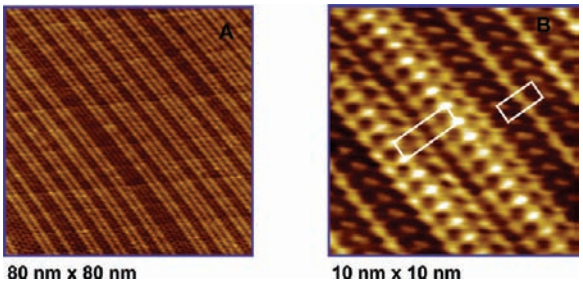

Figure 3. STM images of ceria promoted surface oxidation of Cu(111). (A) A novel structure of a copper oxide was formed by heating a CeO_2/Cu(111) surface in the presence of 5×10^{-7} Torr O_2 at 700 K for 20 min (image size: 80×80 nm^2). The structure of this copper surface oxide is magnified in (B) (image sizes 10×10 nm^2).

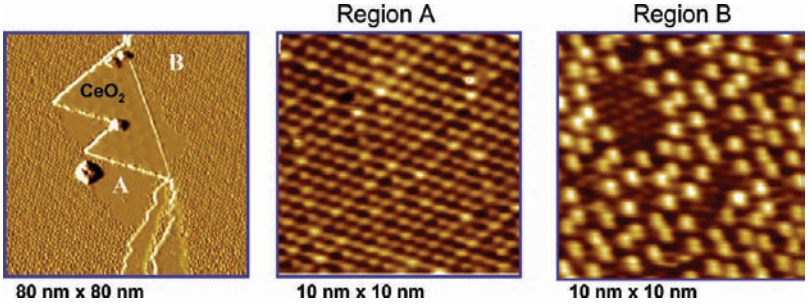

Figure 2. STM images of ceria promoted surface oxidation of Cu(111). The first panel shows a CeO_2/Cu(111) surface that was exposed to 5×10^{-7} Torr O_2 at 550 K for 5 min. The ceria grows forming islands which have triangular shape.[17] Two phases of a Cu_2O oxide are present at the surface and marked as "A" and "B". "A" represents the ordered Cu_2O(111) surface. "B" represents the O-deficient Cu_2O phase. Image sizes are 80×80 nm^2 and 10×10 nm^2.

dx.doi.org/10.1021/ja1087979 |*J. Am. Chem. Soc.* 2011, 133, 3444–3451

Figure 3B, both the bright overlayer oxide rows and the lower oxide surface have a rectangular unit cell. The detailed structure of this Cu_2O_{1+x} surface oxide is still under study. Nonetheless, the growth of the Cu_2O_{1+x} surface oxide clearly suggests the availability of additional atomic oxygen spilling over from ceria.

The question now comes to the nature of ceria sites that facilitates the dissociation of O_2. In Ce 3d XPS spectra, the prepared ceria islands showed the typical line-shape of Ce^{4+}.[16,17] The as prepared or oxidized ceria islands exhibit two overlapping moiré structures, shown in Figure 4. Panels A and B show two honeycomb-type moiré structures, the larger ones (H_1) having a periodicity of ~4.2 nm and the smaller ones (H_2) having a periodicity of 1.20 nm. The inset of Figure 4B shows that H_2 consists of bright dots with ~0.40 nm spacing, corresponding to the lattice of $CeO_2(111)$. The formation of moiré structure is regularly seen in the growth of ultrathin (or two-dimensional) films or nanostructures on a metal surface.[42−44] Because of the lattice mismatch between the supported nanostructure and the substrate, the height of each atom in the supported nanostructure is modulated in order to accommodate it with respect to the substrate lattice and to relief interfacial strain. Consequently, the nanostructure displays a moiré pattern with a periodicity dictated by the coincidence lattice between the supported nanostructure and the substrate. On the oxidized ceria islands, the formation of overlapping moiré structures suggests the existence of two coincidence lattices and thus the presence of a buried phase.

We attribute the buried phase to a thin layer of $Cu_2O(111)$, that is, a O−Cu−O trilayer structure. Figure 2 shows that an ordered (1×1)-$Cu_2O(111)$ surface oxide is formed at the vicinity of ceria islands upon ceria growth at 550 K. The formation of an ordered (1×1)-$Cu_2O(111)$ interfacial layer explains the measured lattice constants of H_1 and H_2. Considering the Cu(111) surface lattice, d_{Cu-Cu} = 0.256 nm, the Cu_2O-(111) surface lattice, d_{O-O} = 0.604 nm, and the $CeO_2(111)$ lattice, d_{Ce-Ce} = 0.389 nm, a coincidence lattice between the $Cu_2O(111)$ and the $CeO_2(111)$ yields a periodicity of 1.208 nm ($3 \times d_{Ce-Ce} = 2 \times d_{O-O}$) if we allow 3.5% expansion of the $CeO_2(111)$ lattice. The contrast modulation of H_2 is thus created by the interference between the $Cu_2O(111)$ interfacial layer and the $CeO_2(111)$ layer, as shown in Figure 4C. Similarly, as the layers of $Cu_2O(111)$ and $CeO_2(111)$ are superimposed onto Cu(111), the lattice mismatch between the Cu(111), Cu_2O-(111), and $CeO_2(111)$ structures creates another contrast modulation, H_1, at the surface of $CeO_2(111)$ (Figure 4D). Note that the crystalline quality of the interfacial $Cu_2O(111)$ layer is dependent on the preparation temperature and O_2 pressure. A defective interfacial $Cu_2O(111)$ layer could cause the distortion of moiré structures, as evidenced in Figure 4B.

3.3. Reaction of CO with CeO_2/Cu_2O_{1+x}/Cu(111). From previous studies, it is known that ceria nanoparticles enhance the adsorption rate of CO on Pt(111) and Rh(111).[7c,d] Figure 5 shows XPS spectrum acquired before and after reducing CeO_2/Cu_2O_{1+x}/Cu(111) with CO. After reduction in 5×10^{-6} Torr of CO at 750 K for 1 h, the Ce 3d XPS spectrum shows that the Ce cations in the supported ceria NPs have been mostly converted into Ce^{3+}.[16] In the STM images of Figure 6, the moiré pattern characteristic of the supported CeO_2 nanoparticles disappeared after reduction in CO and there was a removal of the copper oxide present in areas not covered by ceria in the CeO_2/Cu_2O_{1+x}/Cu(111) system. In Figure 6A, the height difference between the reduced ceria islands and the lower copper terrace is ~3 Å, which corresponds to the height of a "O−Ce−O" trilayer and points to the removal of the Cu_2O layer underneath the ceria islands. Furthermore, under oxidative conditions, the ceria NPs exhibit moiré patterns which are modulated by the interfacial $Cu_2O(111)$ layer. Upon reduction by CO, these patterns disappear, suggesting that the interfacial $Cu_2O(111)$ layer under the ceria NPs was removed. Figure 6B shows that upon reduction ceria NPs exhibit a flat surface with a hexagonal lattice. The lattice spacing is measured at 0.39 nm, corresponding to the lattice of

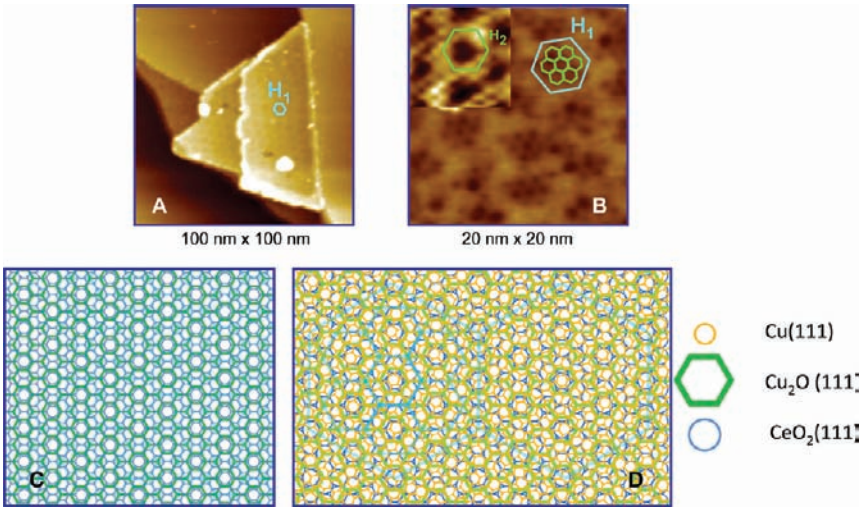

Figure 4. The structure of the oxidized $CeO_2(111)$ nanostructures. (A) STM image of supported $CeO_2(111)$ nanostructures prepared by Ce deposition on Cu(111) in 5×10^{-7} mbar O_2 at 650 K. The surface of $CeO_2(111)$ nanostructures presents a honeycomb-network-type moiré structure (labeled H_1), with a periodicity of ~4.2 nm. The structure underneath H_1 is magnified in (B), showing another hexagonal moiré structure (H_2) with a spacing of 1.2 nm. The structure of H_2 is zoomed in the inset of (B). Image sizes are: (A) 80 × 80 nm^2; (B) 20 × 20 nm^2 (inset: 3 × 3 nm^2). (C and D) The structural illustration of the two moiré structures observed on the oxidized $CeO_2(111)$ nanostructures. The small moiré pattern is caused by the modulation from the underneath $Cu_2O(111)$ layer. The large moiré pattern is modulated by both the underneath $Cu_2O(111)$ layer and the Cu(111) substrate. The blue circles represent Ce atoms in the $CeO_2(111)$ layer. Each vertex of the green hexagons represents oxygen atoms in the $Cu_2O(111)$ layer.

dx.doi.org/10.1021/ja1087979 |J. Am. Chem. Soc. 2011, 133, 3444–3451

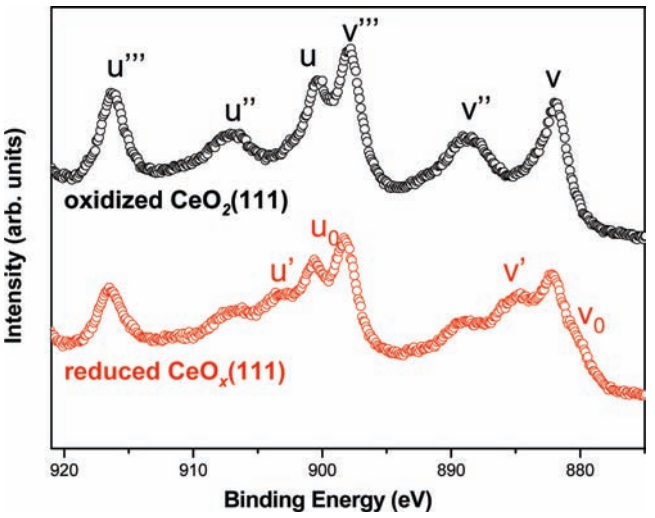

Figure 5. XPS spectra of ceria NPs deposited onto the Cu(111) surface in ~5 × 10^{-7} Torr O_2 at 650 K, followed by annealing in ~5 × 10^{-7} Torr O_2 at 650 K for 20 min (black line), and after reduction in ~5 × 10^{-6} Torr CO at 750 K for 60 min (red line).

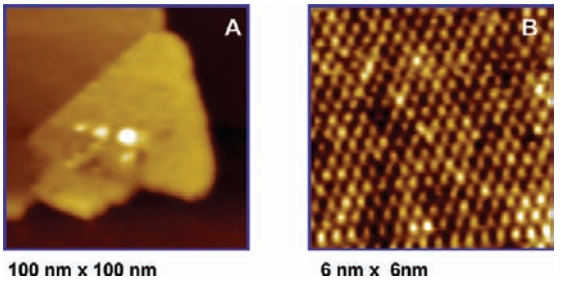

Figure 6. The structure of the reduced CeO_2(111) nanostructures. (A) STM image after reducing the oxidized CeO_2(111) nanostructures in 5 × 10^{-6} Torr CO at 750 K for 60 min. (B) Magnified surface structure of the reduced CeO_2(111), showing a hexagonal lattice with a spacing of 0.39 nm.

CeO_2(111). It is evident now that the ceria on the copper substrate exposes the (111) face. The reduction of the CeO_2 NPs by CO could involve the existence of subsurface oxygen vacancies, which have been observed in multilayer CeO_{2-x}(111) islands in our experiments and in previous studies of bulk CeO_2(111).[45]

XPS studies showed that the reduced ceria NPs could be reoxidized back into Ce^{4+} by reaction with O_2 and reduced again to Ce^{3+} upon further reaction with CO. The corresponding STM study, see Figure 7, found reversibly switching structures for the ceria NPs and the copper oxide layer during redox cycles of exposure to CO and then to O_2. After reoxidation with O_2, the ceria NPs exhibited moiré patterns of the type seen before reduction in CO, with a relative height with respect to the oxidized copper substrate equal to that seen in the initial CeO_2/Cu_2O_{1+x}/Cu(111) systems. Experiments of XPS revealed that at 400−600 K the rate of O_2 dissociation on CeO_x/Cu(111) surfaces produced by the reduction of CeO_2/Cu_2O_{1+x}/Cu(111) was 3−5 times faster than on Cu(111). Figure 8 compares the oxygen uptake on Cu(111) and on a surface in which ceria covered ~15% of the copper substrate. After a dose of 10 L of O_2, all the Ce^{3+} initially present in the CeO_x/Cu(111) surface was transformed into Ce^{4+}. Any additional oxygen that was adsorbed

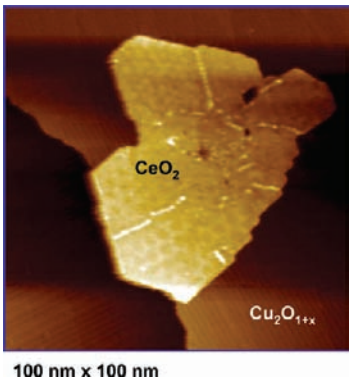

Figure 7. STM image of supported ceria nanostructures after reoxidizing the CeO_{2-x}(111) nanostructures in Figure 6 in ~1 × 10^{-6} Torr O_2 at 750 K for 10 min.

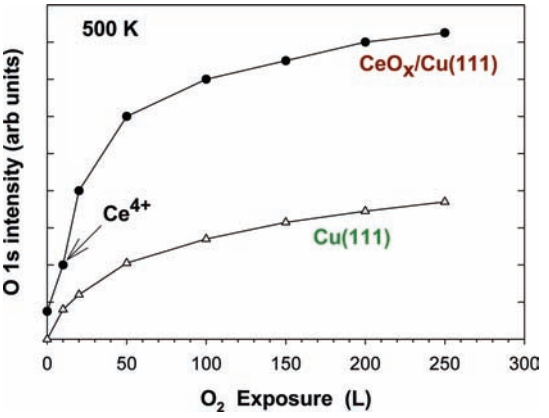

Figure 8. Oxygen uptake on Cu(111) and on a surface in which ceria covered ~15% of the copper substrate. The CeO_x/Cu(111) surface was initially prepared by reducing a CeO_2/Cu_2O_{1+x}/Cu(111) system with CO at 700 K. The Cu(111) and CeO_x/Cu(111) surfaces were exposed to O_2 at 500 K.

ended on the copper forming an oxide layer. These data clearly support the idea that ceria NPs enhance the dissociation of O_2 and the formation of a Cu_2O_{1+x} layer which is not seen for the O_2/Cu(111) system. Since the processes of oxidation in O_2 and reduction in CO are reversible, one may be able to establish a catalytic cycle for the 2CO + O_2 → $2CO_2$ reaction on CeO_x/Cu(111) or CeO_2/Cu_2O_{1+x}/Cu(111).

3.4. CO Oxidation on an Inverse CeO_x/Cu(111) Catalyst. Figure 9 shows Arrhenius plots for CO oxidation on Cu(111) and on a surface in which ceria covered ~18% of the copper substrate (i.e., a system in which O_2 reacts fast with the surface as shown above). In the case of Cu(111), one can estimate turnover frequencies (TOFs) by dividing by the copper surface atom density (1.77 × 10^{15} atoms cm^{-2}).[46] Thus, one obtains TOFs of 0.05 at 475 K and 3.35 at 575 K. These are substantially smaller than TOFs found for CO oxidation on Pt(100), Pt(111), Pd(110), Ir(111), Rh(111), and Ru(0001).[24,47] The inverse CeO_x/Cu(111) catalyst have CO oxidation activities that on a *per area* basis are 20−60 times higher than those of Cu(111). If one takes into consideration that the active sites at the oxide or metal−oxide interface in CeO_x/Cu(111) are at the most 20% of the total number of sites present in Cu(111), then one can estimate TOFs of 6 at 475 K and 990 at 575 K for the oxidation of CO on the inverse CeO_x/Cu(111) catalyst. These TOFs are

dx.doi.org/10.1021/ja1087979 |*J. Am. Chem. Soc.* 2011, 133, 3444–3451

comparable or larger than those reported for surfaces of expensive noble metals such as Rh(111), Pd(110), and Pt(100).[24,47] For example, CeO_x/Cu(111) is a much better catalyst for CO oxidation than Pt(100) or Pt(111).[24] Furthermore, we found that CeO_x/Cu(111) is a good CO oxidation catalyst at relatively low temperatures (325−375 K) where the noble metals do not work well. At these temperatures, the TOFs for CO oxidation on CeO_x/Cu(111) were 4−9 times larger than those measured on Pt(100), Pt(111), and Rh(111).

In Figure 9, the trace for CeO_x/Cu(111) is well fitted by a single straight line that gives an apparent activation energy of 27 kcal/mol. This value is very close to that observed on a Rh(111) catalyst.[48] Postreaction characterization of CeO_x/Cu(111) with XPS and Auger electron spectroscopy showed the presence of $CeO_{1.92-1.96}$ and $CuO_{0.4-0.55}$ on the surface of the catalyst. This agrees with other studies that propose Cu^{1+} cations as an active species during the oxidation of CO in regular and hydrogen-rich (PROX) streams.[2,6] However, Cu_2O also can be generated on Cu(111) but the system does not have high catalytic activity. Thus, the excellent performance of the inverse CeO_x/Cu(111) catalysts is a consequence of the existence of ceria NPs dispersed on a copper oxide support (Figure 7).

3.5. Interaction of O_2 and CO with CeO_x/Cu(111): DFT Studies. In the STM images, triangular CeO_x particles on Cu(111) are shown in both oxidizing and reducing conditions (Figures 4 and 6). Therefore, it seems reasonable that our starting point to build a CeO_x model is a triangular particle made from a CeO_2(111) adsorbed structure on Cu(111). Figure 10 displays our model system. It contains a variable O/Ce ratio depending on interactions with O_2 (oxidative conditions) and CO (reducing conditions). Small particles like this were seen in STM, and our model is also a good representation of the edges of big ceria particles. To avoid the self-interaction of the adsorbed CeO_x particles due to the periodicity, we chose a ($4\sqrt{3} \times 4\sqrt{3}$) Cu(111) surface model. The most stable structure that we found in reducing conditions (as the ones in reaction with pure CO) is a Ce_6O_{13} particle, shown in Figure 10a, where 10 oxygen atoms are in the interface between the plane of Ce atoms and the Cu(111) surface and 3 oxygen atoms are above the Ce plane. The formation energy is +0.57 eV/Ce-atom with respect to the CeO_2 bulk formation energy, but −0.71 eV/Ce with respect to the formation energy of Ce_2O_3 bulk. It is a particle more stable than the bulk of Ce_2O_3 but less stable than the CeO_2 bulk. The fact that it is more stable than the bulk of Ce_2O_3, due to interactions with the copper substrate, helps to explain the facile reduction in CO and the reversibility of the reduction/oxidation cycles seen in the experiments.

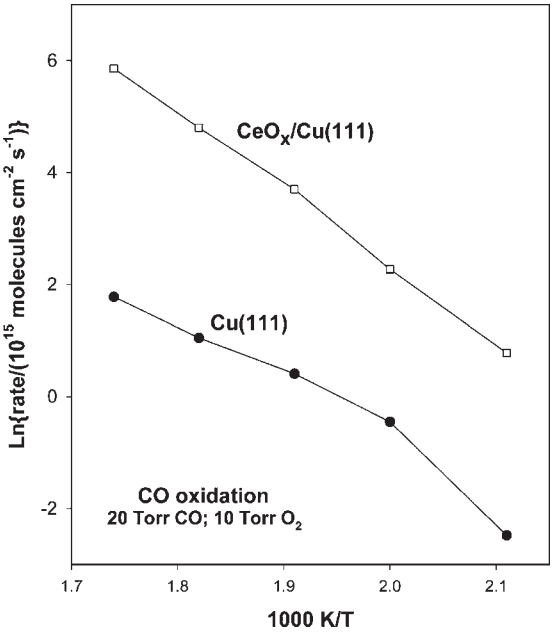

Figure 9. Arrhenius plots for the $2CO + O_2 \rightarrow 2CO_2$ reaction on Cu(111) and on a surface in which ceria covered ∼18% of the copper substrate. P_{CO} = 20 Torr, P_{O2} = 10 Torr. The fraction of Cu(111) covered by ceria was determined using ISS after fully reducing CeO_x/Cu(111) in CO and removing all the CuO_x present.[17]

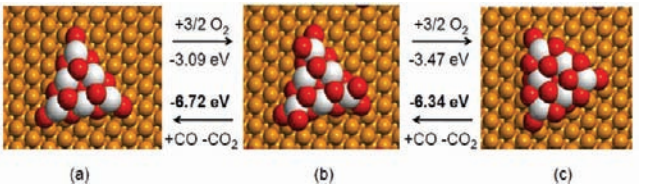

Figure 10. Top view of the optimized structures of the particles (a) Ce_6O_{13}, (b) Ce_6O_{16}, and (c) Ce_6O_{19}. The energies involved in the interconversion by oxidative−reductive cycles with O_2 or CO are shown. Atom colors: Ce (white), O (soft-red), and Cu (gold).

To better understand the interaction between the ceria particle and the support, we performed first a Bader analysis of the charge. There is a charge transfer of 3.96 *e* from the Cu slab to the particle, with 90% of the charge coming from the surface layer. So, there is an oxidation of the Cu surface and a reduction of the particle. The Bader oxidation state of Ce in the particle is +2.00. Since we calculated the Bader charge of Ce in CeO_2 and Ce_2O_3 to be +2.27*e* and +2.02*e*, respectively, and we know the formal oxidation states +4 and +3, respectively, we can extrapolate the Bader oxidation state of Ce in the particle to obtain a formal oxidation state of +2.93. Moreover, there is a high magnetization ∼0.9 in the 4f band of all the Ce atoms. Therefore, despite of the high ratio O/Ce in the particle, we can conclude that all the Ce atoms are formally Ce^{3+}. This is a consequence of oxidation of the Cu atoms at the interface, which means that the O atoms at the interface are shared by Cu and Ce. Therefore, CeO_x/CuO_y represents a real mixed-metal oxide with shared oxygens and unique catalytic properties.

We analyzed also the density of states (DOS) of this system and compared it with the DOS of CeO_2, Ce_2O_3, and Cu_2O bulk (Figure 11). If we compare the DOS projected on Ce and O atoms of the systems CeO_x/Cu(111) and CeO_2 and Ce_2O_3 bulk, we can see that it is a great similarity between the electronic structure of the Ce_2O_3 bulk and that of the CeO_x particle on Cu(111). The 4f band corresponding to Ce^{3+} is stabilized in the particle (moving ∼0.7 eV to lower energies) with respect to the Ce_2O_3 bulk structure, which means that the Ce^{3+} species are more stable in the supported particle than in the Ce_2O_3 bulk and agrees perfectly with the fact that the formation energy of the supported particle is −0.71 eV/Ce-atom with respect to the formation energy of the Ce_2O_3 bulk. If we compare now the DOS of the CeO_x/Cu(111) system with the DOS of the Cu_2O and Ce_2O_3 bulk, we can see that the DOS projected on the O atoms at the interface CeO_x/Cu (O1, O2, O3 in the Figure 11) lies in energies just in between the energies of the DOS projected on O atoms in Cu_2O and Ce_2O_3 bulk. We can say properly that these O atoms at the interface have an intermediate electronic

dx.doi.org/10.1021/ja1087979 |*J. Am. Chem. Soc.* 2011, 133, 3444–3451

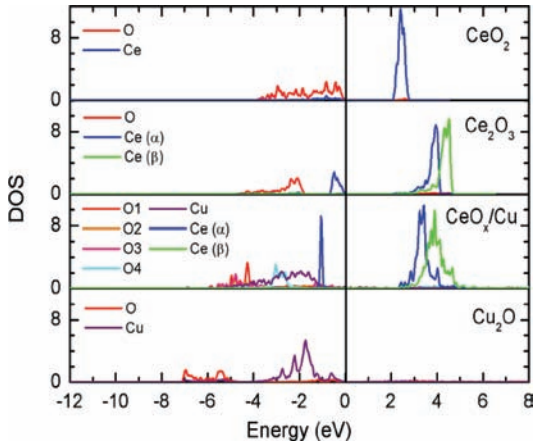

Figure 11. DOS projected on Ce and O atoms of the systems (from top to bottom): CeO_2 bulk, Ce_2O_3 bulk, Ce_6O_{13}/Cu(111) and Cu_2O bulk. O1, O2, O3 are the O atoms of the Ce_6O_{13} particle located at the interface CeO_x/Cu(111). O4 are the O atoms located on top of the Ce_6O_{13} particle. The Cu projected DOS in the CeO_x/Cu system refers to the electronic density of the Cu atoms just under the particle that are sharing the O atoms of the CeO_x particle at the interface. When the α and β electronic densities are represented separately, they are labeled as α and β, respectively (for example, Ce(α) or Ce(β)).

structure between the Cu_2O and Ce_2O_3, as we could expect for a mixed-metal oxide $(Cu,Ce)O_x$. This agrees with the fact that oxygen atoms are interacting simultaneously with oxidized Cu and Ce atoms. At the interface, the presence of a mixed-metal oxide film $(Ce,Cu)O_x$ is seen at the electronic level. However, the projected DOS (PDOS) for the O atoms which are above the Ce plane (O4 in the Figure 11) is more similar to PDOS for the O atoms in the Ce_2O_3 bulk. This is completely coherent with the fact that they are interacting only with Ce^{3+} atoms. Finally, the PDOS on Cu in the CeO_x/Cu and in Cu_2O systems are similar. Only the Cu band is slightly stabilized in the CeO_x/Cu interface with respect to the Cu_2O bulk phase, moving to lower energies.

Now, we can consider the cycle of oxidation−reduction of our particle. For that, we use the following particles: Ce_6O_{13}, Ce_6O_{16}, Ce_6O_{19}. In the Ce_6O_{16} case, we considered two possibilities for the accommodation of the incoming three O atoms starting from the structure of Ce_6O_{13}: on the Ce in the three vertexes or in the Ce in the middle of three sides of the particle. Accommodating the incoming three O atoms in the vertexes of the particle was 1.45 eV more stable than in the middle of the edges. From now on, the particle Ce_6O_{16} will be the one with the extra O atoms in the vertexes of the particle. In the optimization process of the most oxidized one, the particle was rotated itself with respect to the support. The most stable structures found for the 3 particles are shown in the Figure 10. The formation energy of the three particles Ce_6O_{13}, Ce_6O_{16}, Ce_6O_{19} with respect to the CeO_2 bulk are: +0.57, +0.05, −0.52 eV/Ce-atom. So it is obvious that the stability of the supported particle increases with the number of oxygen atoms, becoming even more stable than the CeO_2 bulk. The oxidation states of the Ce atoms are 6 Ce^{3+} in Ce_6O_{13}, 3 Ce^{3+} and 3 Ce^{4+} in the Ce_6O_{16}, and 6 Ce^{4+} in the Ce_6O_{19}. To ensure the stability depending of the oxidizing−reducing conditions, we calculate the energy involve in the oxidation processes of the $Ce_6O_{13} + 3/2O_2 \rightarrow Ce_6O_{16}$, $Ce_6O_{16} + 3/2O_2 \rightarrow Ce_6O_{19}$ and in the reduction processes of $Ce_6O_{19} + 3CO \rightarrow Ce_6O_{16} + 3CO_2$, $Ce_6O_{16} + 3CO \rightarrow Ce_6O_{13} + 3CO_2$. We summarize the results in Figure 10. The dissociative adsorption of O_2 is a very exothermic process. Under a dynamic flow of O_2, one can expect dissociation of a molecule on the ceria, and then the O adatoms can spill over to the copper substrate while their initial place in ceria is covered by the dissociation of a second molecule. By this mechanism, ceria NPs can promote the oxidation of Cu(111).

Furthermore, in Figure 10, the reduction with CO in all cases is much more favored than the oxidation with O_2. This makes possible the closure of a catalytic cycle for CO oxidation. Owing to their special electronic and chemical properties, the supported ceria NPs alone could catalyze the oxidation of CO. However, in the actual process, one could have interaction of adsorbed CO with oxygen directly on top of ceria or on the copper substrate after spillover of the oxygen. The place of reaction will be determined by the rate of adsorption of CO on ceria, copper oxide, or the interface of the oxides. The configuration of the inverse oxide/metal catalysts opens new interesting routes for applications in catalysis[15,49] and it is possible to use it with high-surface area powders.[12] CeO_x NPs also can be added to noble-metal surfaces to enhance their activity for CO oxidation,[7c,d] but these systems seem to behave in a different way with respect to the CeO_x/Cu(111) system where ceria is very efficient for the dissociation of O_2 and accelerates the oxidation of the copper substrate.

4. SUMMARY AND CONCLUSIONS

Cu(111) displays a low activity for the dissociation of O_2 and the oxidation of carbon monoxide. After exposing the surface to O_2, one can get chemisorbed O on Cu(111) or a layer of Cu_2O (the so-called "29" and "44" structures). The addition of ceria NPs to Cu(111) substantially enhances interactions with the O_2 molecule and facilitates the oxidation of the copper substrate. The ceria provides a much faster channel for oxidation than the step edges of Cu(111). After annealing CeO_2/Cu(111) in O_2 at elevated temperatures (600−700 K), a new phase of a Cu_2O_{1+x} surface oxide appears and propagates from the ceria NPs. In images of STM, the ceria NPs are located at ascending step edges surrounded by regions of Cu_2O and Cu_2O_{1+x}. As a consequence of the lattice mismatch between the supported NPs and the copper substrate, the ceria NPs exhibit two overlapping honeycomb-type moiré structures, with the larger ones (H_1) having a periodicity of 4.2 nm and the smaller ones (H_2) having a periodicity of 1.20 nm.

Exposure to CO at 550−750 K led to a partial reduction of the ceria NPs ($Ce^{4+} \rightarrow Ce^{3+}$) and the removal of the copper oxide layer. The reduced ceria islands could be reoxidized back into Ce^{4+} by reaction with O_2 and reduced again to Ce^{3+} upon further reaction with CO. Since the processes of oxidation in O_2 and reduction in CO are reversible, one is able to establish a catalytic cycle for the $2CO + O_2 \rightarrow 2CO_2$ reaction on CeO_x/Cu(111). The CeO_x/Cu(111) systems have activities for the $2CO + O_2 \rightarrow 2CO_2$ reaction that are comparable or larger than those reported for surfaces of expensive noble metals such as Rh(111), Pd(110), and Pt(100). CeO_x/Cu(111) is a good CO oxidation catalyst even at relatively low temperatures (325−375 K) where the noble metals do not work well. Density-functional calculations show that the supported ceria NPs are able to catalyze the oxidation of CO due to their special electronic and chemical properties. The inverse CeO_x/Cu(111) catalyst illustrates the important role that ceria can play in CO oxidation processes.

dx.doi.org/10.1021/ja1087979 |J. Am. Chem. Soc. 2011, 133, 3444–3451

AUTHOR INFORMATION

Corresponding Author
rodrigez@bnl.gov

ACKNOWLEDGMENT

The work performed at BNL was supported by the U.S. Department of Energy, Office of Basic Energy Sciences, under contract DE-AC02-98CH10886. J.E. is grateful to INTEVEP and IDB for partial support of the work carried out at the UCV. The work done at Seville was funded by MICINN, grant no. MAT2008-04918 and Barcelona Supercomputing Center − Centro Nacional de Supercomputación (Spain).

REFERENCES

(1) Jernigan, G. G.; Somorjai, G. A. *J. Catal.* **1994**, *147*, 567.
(2) Gamarra, D.; Belver, C.; Fernández-García, M.; Martínez-Arias, A. *J. Am. Chem. Soc.* **2007**, *129*, 12064.
(3) (a) Szanyi, J.; Goodman, D. W. *Stud. Surf. Sci. Catal.* **1993**, *75*, 1599. (b) Domagala, M. E.; Campbell, C. T. *Catal. Lett.* **1991**, *9*, 65.
(4) Newsome, D. S. *Catal. Rev. Sci. Eng.* **1980**, *21*, 275.
(5) Rao, K. N.; Bharali, P.; Thrimurthulu, G.; Reddy, B. *Catal. Commun.* **2010**, *11*, 863.
(6) Huang, T.-J.; Tsai, D.-H. *Catal. Lett.* **2003**, *87*, 173.
(7) (a) McClure, S. M.; Goodman, D. W. *Chem. Phys. Lett.* **2009**, *469*, 1. (b) Xu, J.; While, T.; Li, P.; He, C.; Yu, J.; Yuan, W.; Han, Y.-F. *J. Am. Chem. Soc.* **2010**, *132*, 10398. (c) Suchorski, Y.; Wrobel, R.; Becker, S.; Weiss, H. *J. Phys. Chem. C* **2008**, *112*, 20012. (d) Eck, S.; Castellarin-Cudia, C.; Surnev, S.; Prince, K. C.; Ramsey, M. G.; Netzer, F. P. *Surf. Sci.* **2003**, *536*, 166.
(8) Park, J. B.; Graciani, J.; Evans, J.; Stacchiola, D.; Ma, S; Liu, P.; Nambu, A.; Sanz, J. F.; Hrbek, J.; Rodriguez, J. A. *Proc. Natl. Acad. Sci. U. S.A.* **2009**, *106*, 4975.
(9) Valden, M.; Lai, X.; Goodman, D. W. *Science* **1998**, *281*, 1647.
(10) (a) Gong, J. L.; Ojifinni, R. A.; Kim, T. S.; White, J. M.; Mullins, C. B. *J. Am. Chem. Soc.* **2006**, *128*, 9012. (b) Gong, J. L.; Ojifinni, R. A.; Kim, T. S.; Stiehl, J. D.; McClure, S. M.; White, J. M.; Mullins, C. B. *Top. Catal.* **2007**, *44*, 57.
(11) Zheng, X.; Wang, S.; Wang, Sh.; Zhang, S.; Huang, W.; Wu, S. *Catal. Commun.* **2004**, *5*, 729.
(12) Homés, A.; Hungría, A. B.; Bera, P.; López Cámara, A.; Fernández-García, M.; Martínez-Arias, A.; Barrio, L.; Estrella, M.; Zhou, G.; Fonseca, J. J.; Hanson, J. C.; Rodriguez, J. A. *J. Am. Chem. Soc.* **2010**, *132*, 34.
(13) Snytnikov, P. V.; Popova, M. M.; Men, Y.; Rebrov, E. V.; Kolb, G.; Hessel, V.; Schouten, J. C.; Sobyanin, V. A. *Appl. Catal., A* **2008**, *350*, 53.
(14) *Catalysis by Ceria and Related Materials*; Trovarelli, A., Ed.; World Scientific: London, 2002.
(15) Rodriguez, J. A.; Hrbek, J. *Surf. Sci.* **2010**, *604*, 241.
(16) Rodriguez, J. A.; Ma, S.; Liu, P.; Hrbek, J.; Evans, J.; Pérez, M. *Science* **2007**, *318*, 1757.
(17) Rodriguez, J. A.; Graciani, J.; Evans, J.; Park, J. B.; Yang, F.; Stacchiola, D.; Senanayake, S. D.; Ma, S.; Pérez, M.; Liu, P.; Sanz, J. F.; Hrbek, J. *Angew. Chem., Int. Ed.* **2009**, *48*, 8047.
(18) Matsumoto, T.; Bennett, R. A.; Stone, P.; Yamada, T.; Domen, K.; Bowker, M. *Surf. Sci.* **2001**, *471*, 225.
(19) Jensen, F.; Besenbacher, F.; Laegsgaard, E.; Stensgaard, I. *Surf. Sci.* **1991**, *259*, L774.
(20) Jensen, F.; Besenbacher, F.; Stensgaard, I. *Surf. Sci.* **1992**, *270*, 400.
(21) Soon, A.; Todorova, M.; Delley, B.; Stampfl, C. *Phys. Rev. B* **2006**, *73*, 165424–12.
(22) Yang, F.; Choi, Y.-M.; Liu, P.; Hrbek, J.; Rodriguez, J. A. *J. Phys. Chem. C* **2010**, *114*, 17042.
(23) Liu, G.; Rodriguez, J. A.; Chang, Z.; Hrbek, J.; Peden, C. H. F. *J. Phys. Chem. B* **2004**, *108*, 2931.
(24) Berlowitz, P. J.; Peden, C. H. F.; Goodman, D. W. *J. Phys. Chem.* **1988**, *92*, 5213.
(25) Kresse, G.; Joubert, J. *Phys. Rev. B* **1999**, *59*, 1758.
(26) Perdew, J.; Chevary, J.; Vosko, S.; Jackson, K.; Pederson, M.; Singh, D.; Fiolhais, C. *Phys. Rev. B* **1992**, *46*, 6671.
(27) Kresse, G.; Hafner, J. *Phys. Rev. B* **1993**, *47*, 558–561.
(28) Kresse, G.; Furthmuller, J. *Comput. Mater. Sci.* **1996**, *6*, 15–50; *Phys. Rev. B* **1996**, *54*, 11169–11186.
(29) Dudarev, S. L.; Botton, G. A.; Savrasov, S. Y.; Humphreys, C. J.; Sutton, A. P. *Phys. Rev. B* **1998**, *57*, 1505.
(30) Fabris, S.; de Gironcoli, S.; Baroni, S.; Vicario, G.; Balducci, G. *Phys. Rev. B* **2005**, *72*, 237102.
(31) Cococcioni, M.; de Gironcoli, S. *Phys. Rev. B* **2005**, *71*, 035105.
(32) Castleton, C. W. M.; Kullgren, J.; Hermansson, K. *J. Chem. Phys.* **2007**, *127*, 244704.
(33) Andersson, D. A.; Simak, S. I.; Johansson, B.; Abrikosov, I. A.; Skorodumova, N. V. *Phys. Rev. B* **2007**, *75*, 035109.
(34) Nolan, M.; Grigoleit, S.; Sayle, D. C.; Parker, S. C.; Watson, G. W. *Surf. Sci.* **2005**, *576*, 217.
(35) Nolan, M.; Parker, S. C.; Watson, G. W. *Surf. Sci.* **2005**, *595*, 223.
(36) Nolan, M.; Parker, S. C.; Watson, G. W. *J. Phys. Chem. B* **2006**, *110*, 2256–2262.
(37) Watkins, M. B.; Foster, A. S.; Shluger, A. L. *J. Phys. Chem. C* **2007**, *111*, 15337–15341.
(38) Yang, Z.; Lu, Z.; Luo, G. *Phys. Rev. B* **2007**, *76*, 075421.
(39) Da Silva, J. L. F. *Phys. Rev. B* **2007**, *76*, 193108.
(40) Da Silva, J. L. F.; Ganduglia-Pirovano, M. V.; Sauer, J.; Bayer, V.; Kresse, G. *Phys. Rev. B* **2007**, *75*, 045121.
(41) Wiame, F.; Maurice, V.; Marcus, P. *Surf. Sci.* **2007**, *601*, 1193.
(42) Gritschneder, S.; Becker, C.; Wandelt, K.; Reichling, M. *J. Am. Chem. Soc.* **2007**, *129*, 4925.
(43) Cisternas, E.; Flores, M.; Vargas, P. *Phys. Rev. B* **2008**, *78*, 5.
(44) Marchini, S.; Gunther, S.; Wintterlin, J. *Phys. Rev. B* **2007**, *76*, 9.
(45) Torbrugge, S.; Reichling, M.; Ishiyama, A.; Morita, S.; Custance, O. *Phys. Rev. Lett.* **2007**, *99*, -.
(46) Nakamura, J.; Campbell, J. M.; Campbell, C. T. *J. Chem. Soc., Faraday Trans.* **1990**, *86*, 2725.
(47) Rodriguez, J. A.; Goodman, D. W. *Surf. Sci. Rep.* **1991**, *14*, 1.
(48) Goodman, D. W.; Peden, C. H. F. *J. Phys. Chem.* **1986**, *90*, 4839.
(49) Matolin, V.; Libra, J.; Skoda, M.; Tsud, N.; Prince, K. C.; Skala, T. *Surf. Sci.* **2009**, *603*, 1087.